APL Materials

Metal–organic chemical vapor deposition of 2D van der Waals materials—The challenges and the extensive future opportunities

Cite as: APL Mater. **8**, 030901 (2020); https://doi.org/10.1063/1.5142601
Submitted: 15 December 2019 . Accepted: 13 February 2020 . Published Online: 02 March 2020

Do Hee Lee, Yeoseon Sim, Jaewon Wang, and Soon-Yong Kwon

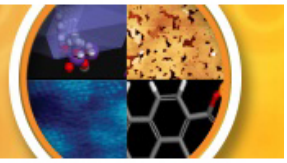

Metal–organic chemical vapor deposition of 2D van der Waals materials—The challenges and the extensive future opportunities

Cite as: APL Mater. 8, 030901 (2020); doi: 10.1063/1.5142601
Submitted: 15 December 2019 • Accepted: 13 February 2020 •
Published Online: 2 March 2020

Do Hee Lee, Yeoseon Sim, Jaewon Wang, and Soon-Yong Kwon[a)]

AFFILIATIONS

School of Materials Science and Engineering and Center for Future Semiconductor Technology (FUST), Ulsan National Institute of Science and Technology (UNIST), Ulsan 44919, South Korea

[a)]Author to whom correspondence should be addressed: sykwon@unist.ac.kr

ABSTRACT

The last decade has witnessed significant progress in two-dimensional van der Waals (2D vdW) materials research; however, a number of challenges remain for their practical applications. The most significant challenge for 2D vdW materials is the control of the early stages of nucleation and growth of the material on preferred surfaces to eventually create large grains with digital thickness controllability, which will enable their incorporation into high-performance electronic and optoelectronic devices. This Perspective discusses the technical challenges to be overcome in the metal–organic chemical vapor deposition (MOCVD) growth of 2D group 6 transition metal dichalcogenide (TMD) atomic crystals and their heterostructures, as well as future research aspects in vdW epitaxy for 2D TMDs via MOCVD. In addition, we encourage the traditional MOCVD community to apply their expertise in the field of "2D vdW materials," which will continue to grow at an exponential rate.

INTRODUCTION

Electronic and optoelectronic devices based on layered two-dimensional transition metal dichalcogenides (2D TMDs) feature unique properties that yield outstanding figures of merit. Diverse TMDs (e.g., MoS_2, WSe_2, WTe_2, SnS_2, and ReS_2) can be obtained through the deliberate selection of both the TM and chalcogen atoms, and their versatile and tunable properties permit a wide degree of control for on-demand heterojunction device design.[1–7] Pioneering research has already demonstrated related proof-of-concept transistors and memory cells for ultra-low power electronics, in addition to photodetectors, photodiodes, light-emitting diodes (LEDs), and solar cells as high-quantum-efficiency optoelectronics using 2D group 6 TMDs such as (Mo, W) (S, Se, $Te)_2$, as shown in Table I.[8–19]

For digital logic transistors, the sizable bandgaps of such TMDs are beneficial for a high on/off ratio, and their extreme thinness enables more effective switching and reduction of short-channel effects and power dissipation. Radisavljevic *et al.* first fabricated the top-gated MoS_2-monolayer-based transistor with a room-temperature (RT) mobility of >200 $cm^2\ V^{-1}\ s^{-1}$, high on–off ratio of ~10^8, and a subthreshold swing of ~74 mV/decade.[8] The top-gated geometry and the high-κ dielectric HfO_2 can enhance the performance of MoS_2 transistors. Furthermore, because the stacked structure based on 2D materials having semiconducting, insulating, and metallic properties facilitates control of carrier doping concentration and polarity in TMDs, the TMD-based stacked structures have been utilized in memory devices such as floating gate transistors and ferroelectric-gate field effect transistors (FETs). Vu *et al.* demonstrated a two-terminal floating-gate memory, which is composed of a monolayer MoS_2/h-BN/monolayer graphene vertical stack.[10] Control of the insulating layer thickness (<10 nm) facilitates charge tunneling to the floating layer. The memory device exhibited an ultralow off-state current of 10^{-14} A and an ultrahigh on/off ratio of >10^9. Due to the absence of a rigid dielectric layer, the device can stretch up to a strain of ~19% without electrical performance degradation.

TABLE I. Applications of TMD-based devices (fabricated by mechanical exfoliation).

Industry	Device requirement	Application	Material	Structure	Performance	Material attribution	References
Electronics	Low power consumption Excellent short channel control	Transistor	MoS_2	Au/Cr(top gate)/ HfO_2(dielectric layer)/ Au(electrodes)/ 1L MoS_2 (exfoliated)/ SiO_2/Si	200 cm^2 V^{-1} s^{-1} at RT, high on–off ratio (10^8), and ultralow standby power dissipation (74 mV dec for a bias V_{ds} = 100 mV, I_{off} ≈25 fA μm^{-1})	Transparent semiconducting material (MoS_2: 6.5 Å, WSe_2: 7.0 Å) Large intrinsic direct bandgap (MoS_2:1.8 eV, WSe_2:1.62 eV) High thermal stability Absence of dangling bonds	8
			WSe_2	Au/Ti(top gate)/ HfO_2(dielectric layer)/ Au/Ti(electrodes)/ 1L WSe_2(exfoliated)/ HfO_2(dielectric layer)/p + Si(back gate)	250 cm^2 V^{-1} s^{-1} at RT, high on–off ratio (10^6), and ultralow standby power dissipation (~60 mV dec for a bias V_{ds} = 500 mV, I_{off} ≈ 11 fA μm^{-1})		9
		Memory	MoS_2	Au/Cr(electrodes)/ 1L MoS_2(exfoliated)/ h-BN/Graphene(CVD)/ PET	Ultimately low off-state current of 10^{-14}, ultrahigh on/off ratio over 10^9, and high stretchability (>19%)		10
			WSe_2	Au/Cr(electrodes)/ WSe_2(exfoliated)/ MoS_2(exfoliated) -h-BN(exfoliated)/ $HfS_2/Al_2O_3/Si$	Quasi-non-volatile RAM technology, ultrahigh-speed writing operation (approximately 15 ns) approximately 10^6 times faster than other memories based on 2D materials, and long refresh time to 10 s		11
		Photodetector	MoS_2	Au(electrodes)/ 1L MoS_2(exfoliated) /SiO_2/Si	Photoresponsivity of 880 A W^{-1} at 561 nm and photoresponse in the 400–680 nm, range		12
			WSe_2	Au/Pd(electrodes)/ 1L WSe_2(CVD)/SiO_2/Si	Photoresponsivity of ~1.8 × 10^5 A W^{-1}		13
			MoS_2	Ti(electrode)/ 50 nm MoS_2(exfoliated)/ Graphene(CVD) (electrode)/ Al_2O_3(dielectric layer)/ ITO(back gate)/Glass	External quantum efficiency (EQE) of 55% and internal quantum efficiency (IQE) up to 85%		14

TABLE I. (*Continued.*)

Industry	Device requirement	Application	Material	Structure	Performance	Material attribution	References
Optoelectronics	Highly efficient photocurrent generation Efficient electron–hole pair generation High photoresponsivity	Photodiode	WSe_2	Au(or Au//Pd, electrodes)/ 1L WSe_2(exfoliated)/ HfO_2/Au(or AuPd, two local gates)/SiO_2/Si	Photodetector, photoresponsivity of 210 mA W^{-1}, solar cell, external quantum efficiency (EQE) of 0.2%, at 522 nm LED, and electroluminescence peak at 752 nm	Near-infrared to visible bandgap Strong exciton binding energy (MoS2: ~0.55 eV, WSe2: ~0.45 eV) Mainly based on photovoltaic effect Low dark current	15
			MoS_2/WSe_2	Graphene/MoS_2/ WSe_2/Graphene [all Graphene(Gr), MoS_2, and WSe_2 are prepared by mechanical exfoliation.]	Zero-bias responsivity of ~10 mA/W and high EQE of ~10%–30%		16
		LED	MoS_2	hBN/Gr/hBN/MoS_2/hBN/ MoS_2/hBN/MoS_2/hBN/ Gr/hBN/SiO_2/Si [all Graphene(Gr), hBN, and MoS_2 are prepared by mechanical exfoliation.]	Multiple quantum wall(MQW) devices. Quantum efficiency (QE) of MoS2: ~8.4% (for the device with quadruple QW)		17
			WSe_2	Au/V(electrodes)/ 1L WSe_2(exfoliated)/ hBN/Pd(two local gates)/ SiO_2/Si	Lateral p–n junction and bright electroluminescence with 1000 times smaller injection current and 10 times smaller electroluminescence linewidth than in MoS_2		18
		Solar cell	MoS_2/WSe_2	Pd/Au(electrodes)/ 1L MoS_2(exfoliated)/ 1L WSe_2(exfoliated)/ Si/SiO_2(back gate)	EQE of 1.5%, fill factor(FF) of 0.5, and power conversion efficiency (PCE) of ~0.2%		19

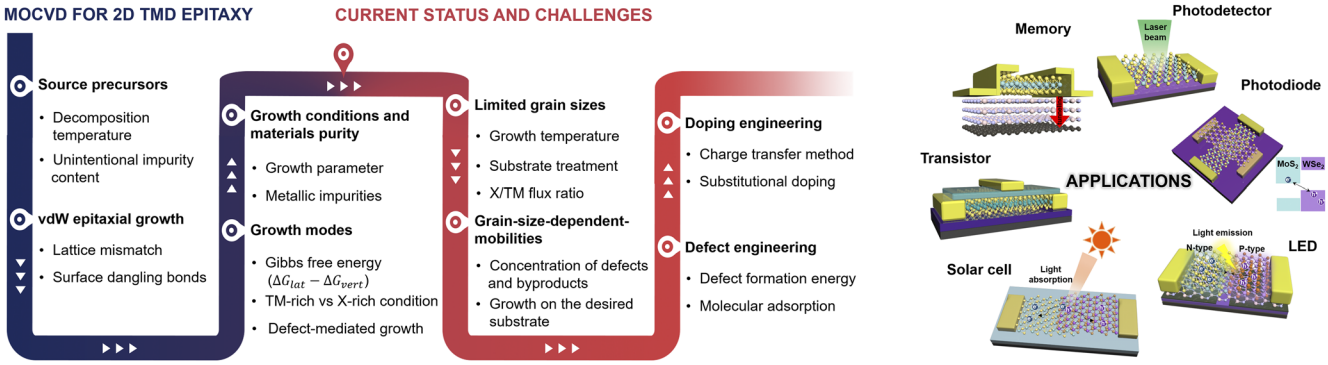

FIG. 1. Recent development of 2D TMD epitaxy by MOCVD.

The direct bandgaps of TMDs from the near-infrared region to the visible region also make them effective in optoelectronic applications.[2] Moreover, based on theoretical calculations, diverse monolayer TMDs have considerably high exciton binding energies (~0.5–1 eV).[20,21] The 2D TMD-based devices are expected to be utilized in RT optoelectronic devices. In the case of photodetectors, because of the sizable energy gap, TMD-based photodetectors can have lower dark current and higher responsivity than zero-bandgap graphene-based photodetectors. However, extremely strong excitonic effects hinder effective exciton dissociation by electric fields, demanding a large bias electric field. To overcome the intrinsic problem and improve the performance of MoS_2-based photodetectors, Lopez-Sanchez *et al.* achieved improvement in semiconductor–metal contacts and mobility of MoS_2.[12] The proposed device exhibited a high photoresponsivity of 880 A/W at 561 nm and a broad photoresponse over the 400–680 nm range. For more controllable and efficient photodetectors, in-plane and out-of-plane junctions have been demonstrated. Baugher *et al.* fabricated a monolayer-WSe_2-based photodetector with an in-plane *p*–*n* junction, which is controlled by electrostatic gates.[15] The device exhibited a photodetection responsivity of ~1 and ~210 mA/W under zero bias and large forward bias, respectively. However, the external quantum efficiency (EQE) was very low (~0.2%) because of the limitation of the in-plane junction in a wide depletion region. For an out-of-plane *p*–*n* junction, Lee *et al.* demonstrated a MoS_2/WSe_2 vertical heterostructure.[16] Owing to the large-area depletion region, the device exhibited a high zero-bias responsivity of ~10 mA/W and a higher EQE of ~10%–30%. In the case of excitonic LEDs, Ross *et al.* reported a monolayer WSe_2 in-plane *p*–*n* diode and demonstrated that the electroluminescence among the regimes of impurity-bound, charged, and neutral excitons is tunable with the change in the injection bias.[18] In the case of thin-film solar cells, Furchi *et al.* demonstrated the photovoltaic effect of a MoS_2/WSe_2 vertical vdW heterojunction.[19] Through the electrical tuning of WSe_2 from *n*-type to *p*-type, the MoS_2/WSe_2 heterostructure can obtain the *p*–*n* junction, resulting in a EQE of ~1.5%, a fill factor of ~0.5, and a power conversion efficiency of ~0.2%.

As shown in the examples above, combined experimental and theoretical studies on these vdW materials have increased rapidly in recent years. The appeal of 2D materials lies in their layered vdW nature with no covalent bonding between a grown vdW material and the substrate.[22–25] This bonding nature of the 2D materials allows the choice of materials systems based primarily on "bandgap engineering" (i.e., artificial modification of band-edge profiles using heterostructures by epitaxial growth) without any epitaxial matching requirements. This provides great flexibility for fabricating on-demand heterostructures with desired properties. However, despite the tremendous potential for novel applications, the controllable synthesis of continuous and homogeneous 2D TMDs at the wafer-scale remains quite challenging.[7] Specifically, it should be noted that most of the observed novel electrical and optoelectronic properties have been demonstrated in exfoliated TMD flakes.[8–19] The chemical vapor deposition (CVD) may be used to perform the large-scale synthesis of high-quality 2D TMDs[26–30] and their heterostructures.[31–33] Nonetheless, the commonly used powder vaporization routes (e.g., MoS_2 from MoO_3 and S powders) require high growth temperatures and are limited in terms of continuous and constant supply of precursors during growth,[7,26–30] making them unsuitable for integration into existing electronic manufacturing processes. The development of a reliable large-scale synthesis process would unleash the potential of 2D TMDs in electronic and optoelectronic applications and may trigger the development of novel and unexpected uses, where their unique properties could produce significant enhancements. From this perspective, metal–organic CVD (MOCVD) that can address these scalability and process control issues during the vapor-phase growth of 2D TMD atomic crystals will be investigated in this paper (Fig. 1). The focus is to (i) summarize the key technologies used for the MOCVD growth of 2D TMDs, (ii) highlight the potential of the MOCVD process while discussing its drawbacks, (iii) discuss many challenges that remain to be overcome for realizing practical applications of 2D TMD by MOCVD, and (iv) encourage the traditional MOCVD community to apply their expertise in the field of "2D vdW materials," which will continue to grow at an exponential rate.

MOCVD FOR 2D TMD EPITAXY

An excellent review of MOCVD processing technology and its history can be found in Refs. 34 and 35, but a short summary of 2D

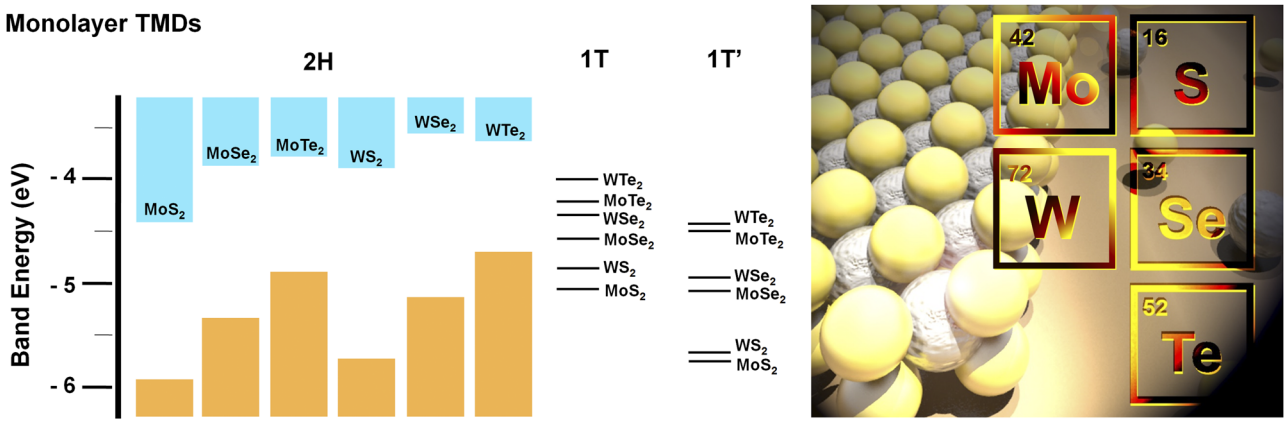

FIG. 2. Band alignment between 2D semiconductors and metals. Left column shows the relative valence and conduction band edges of 2D group 6 monolayer TMDs such as (Mo, W) (S, Se, Te)$_2$. Bars show the work function for 2D TMD metals. The phases are labeled on top of the corresponding columns. Left column and bars are reproduced with permission from Liu *et al.*, Sci. Adv. **2**, e1600069 (2016). Copyright 2016 American Association for the Advancement of Science.

vdW materials, focusing on 2D group 6 semiconducting 2H-TMDs, such as (Mo, W) (S, Se)$_2$ is included herein (Fig. 2). Based on its early commercial use in III–V (or II–VI) compound semiconductor technologies, MOCVD is an emerging technique for the production of wafer-scale and high-quality electronic and optoelectronic materials and their related heterostructures.[34,35] Interest has recently been developed in extending this technique to the growth of 2D vdW materials for various electronic and optoelectronic applications.[36–46] The appeal of MOCVD is because it is readily transportable and is composed high purity organometallic (MO) compounds that can be prepared for most of elements that are of interest for the deposition of 2D TMD materials.[47–49] Furthermore, the large driving force for the pyrolysis of the source chemicals (i.e., large free energy change)[50] indicates that a wide variety of 2D TMD materials can be grown using this technique that cannot be grown using other techniques. In principle, the large free energy change allows the growth of single-crystal-like 2D TMD materials free of grain boundaries (GBs) on various substrates.

Meanwhile, the importance of extreme precision, control, uniformity, and purity required for the efficient operation of optoelectronic devices (e.g., detectors and advanced photonic array devices) has resulted in the continued importance of molecular beam epitaxy (MBE) (over MOCVD) because of the remaining limitations of MOCVD in terms of its relatively high impurity and defect levels.[47–50] MBE has several advantages including high purity, slow growth rate, and *in situ* characterization techniques available under ultrahigh vacuum (UHV), which make it ideal for the study of the vdW epitaxy phenomenon. However, the required purity of TM source materials especially for Mo and W for 2D group 6 TMDs ≈99.95%, while for most other materials, it is ≈ 99.999%.[51] It should be noted that impurity incorporation in most grown films is determined by the purity of starting source materials for the most part. Emerging vdW technology has used MBE for initial device demonstrations,[52–56] although considerable work is being performed to render MOCVD useful for the fabrication of these devices. For TMD growth, TM halides including (W, Mo)Cl$_5$ were used in low-temperature processes, with several examples of atomic layer deposition (ALD).[57–60] However, the ALD routes generally do not produce crystalline TMD materials and remain in their infancy.[57–63]

Source precursors

MOCVD is a nonequilibrium growth technique that relies on the vapor transport of precursors and subsequent chemical reactions in a heated zone.[47–50] Currently, the sources used for major vdW film constituents in MOCVD include various combinations of hydrides and other compounds. The 2D TMD compounds or alloys are usually grown using TM hexacarbonyls or chlorides {e.g., molybdenum hexacarbonyl [Mo(CO)$_6$] or molybdenum chloride (MoCl$_5$)$_2$} as the TM source. By strict definition, these materials are not MOs because an MO indicates the presence of a metal directly bonded via a metal–C bond to an organic fragment.[64] The non-metal source is a hydride (H$_2$S and H$_2$Se) or an MO such as dimethyl sulfide [DMS (CH$_3$)$_2$S] or diethyl sulfide [DES (C$_2$H$_5$)$_2$S].

During MOCVD, the sources are introduced as vapor phase constituents into a growth chamber at approximately RT and thermally decomposed at elevated temperatures using a hot substrate/susceptor to form the vdW film.[47–50,64] The above-mentioned metal precursors are often pyrophoric and exhibit relatively high vapor pressures from ~0.1 Torr to 100 Torr at approximately RT. Therefore, the materials can be easily transported to the growth chamber as vapor phase species by bubbling with a suitable carrier (e.g., H$_2$ or N$_2$). The temperature at which the precursors begin to decompose is a function of the contact surface with the precursor contact and the ambient gas.[50,64] Decomposition is also affected by the residence time of the chemical species around the hot substrate/susceptor surface, indicating a flow rate and reactor geometry dependence of thermal decomposition.[50,64] The reported decomposition temperatures ranged less than ~400 °C for most metal precursors,[7] which is beneficial for the future CMOS-compatible semiconductor industry considering the incorporation of TMDs with the reduced growth temperatures for vdW epitaxy to ≤450 °C.

Apart from the vapor pressure and decomposition temperature, other considerations for the choice of precursors include toxicity and the unintentional impurity content including carbon and oxygen incorporated in the vdW films (i.e., potential sources of defects and dopants).[47–50] During the growth of 2D TMD compounds, hydrides are often used as sources because they are relatively inexpensive and available as dilute vapor phase mixtures at various concentrations. In addition, these precursors eliminate some of the concerns regarding carbon incorporation. However, all hydrides are extremely toxic, and safety costs may exceed material cost savings.[50] Generally, the high toxicity of commonly used hydrides (e.g., H_2S or H_2Se) leads to the substitution of MO compounds (e.g., DMS or DMSe) for hydrides. Besides the toxicity, considering the growth of TMD alloys containing S and Se at temperatures of ≤450 °C, the difference in decomposition temperatures of H_2S and H_2Se complicates the compositional control at low substrate temperatures, driving the movement to MO precursors from S and Se.[65] In addition, the use of DMSe instead of H_2Se for Se-based compounds allowed the minimization of the parasitic gas phase reaction between the Lewis acid and base sources.

vdW epitaxial growth

In traditional 3D Si and III–V (or II–VI) semiconductor systems, an important parameter governing the epitaxial growth is lattice mismatch as it results in strain and defects that restrict the viable material combinations during the formation of on-demand heterostructures.[50] The lattice mismatch originates from the dangling bonds at the surface of the 3D crystalline substrates. In contrast with conventional 3D epitaxy, vdW epitaxy leverages the epilayer and/or the substrate with a vdW surface containing no dangling bonds, as in the epitaxial growth of Se on cleaved bulk Te crystals[22] (lattice mismatch ~20%) as well as F-terminated 3D CaF_2, upon which an ultrathin MoS_2 was grown[66] (lattice mismatch ~17%). Because of the lack of surface dangling bonds, no covalent and/or ionic bonding occurs between the epilayer and substrate. Therefore, when the epitaxial layer is formed on a lattice-mismatched substrate, it grows unstrained with its natural lattice constant, resulting in strain-free growth of the epilayer with atomically abrupt interfaces. Because no strain exists in these hetero-systems, the misfit dislocations will not form, resulting in device quality interfaces despite large lattice mismatch. For atomically thin MoS_2 grown on graphene by CVD, Raman spectra, synchrotron X-ray scattering, and atomic-resolution scanning tunneling microscopy (STM) showed no evidence of strain in the hetero-system, despite the lattice mismatch of ~28%.[67] However, the nucleation and growth process on the substrate with a pristine vdW surface (i.e., containing no dangling bonds) is very difficult due to the weak vdW energy.[68,69]

Growth modes

The classical theory of thin film growth was originally developed to describe the epitaxial growth of 3D materials (i.e., non-vdW materials) containing actual chemical bonds between the growing film and substrate; this is where strain is more influential.[50] All three classical 3D growth modes can be understood from the perspective of the critical radius and free energy barrier for nucleation and growth of the cap-shaped meniscus. However, the treatment of all three modes at once (differentiated by various surface tension inequalities) ignores the actual morphology of the TMD films. This morphology is never cap-shaped, adopting either a single layer or multiple layers without strong bonding between the layers. Therefore, a more constructive approach involves the analysis of the Gibbs free energy change upon formation of nuclei in a manner that explicitly recognizes the layer structure of TMDs (no wetting angle theta) and lateral growth that can increase/widen the first layer or vertical growth that can add a stacked layer.

A revised theory that is specifically tailored for the case of layered vdW atomic crystals grown using vdW substrates was recently proposed by our group [Fig. 3(a)].[7] Regarding nucleation at the early stages of deposition, it is worthwhile to note that the energy barrier (ΔG^*) is always positive (i.e., TMD growth always encounters a barrier to nucleation), and it is an increasing function of n for an n-layer nucleus, implying that all the TMD nuclei formed at the beginning of the growth are monolayer domains, not multilayer ones. Furthermore, an energetic comparison between the lateral and vertical growth modes of TMDs was carried out, and the thermodynamically favored configuration (lateral or vertical) is written as $\Delta G_{lat} - \Delta G_{vert} = a_2 r_2^2(\varepsilon_{12} - \varepsilon_{02}) - l(\lambda_1 + \lambda_2 - \lambda_i)$, where ε is the binding energy per unit area, l is a length at the 1D interface between nuclei, and λ is an edge formation energy. The numeric subscripts denote the substrate (0) and TMD layers (1 is first, and n is farthest from the substrate). For lateral (vertical) growth to be preferred, the above equation has to be negative (positive). This result indicates a size-dependent thermodynamic criterion for the lateral (or vertical) growth to occur, which opens up several different avenues for growth.

Although some of the highest quality TMD monolayers were synthesized via MOCVD,[36–46,70–81] the common observation of triangular-shaped TMD islands in vdW epitaxy implies inversion symmetry breakage associated with the equilibrium crystal structure.[82–87] This incorrect symmetry possibly indicates different types of defect-mediated growth, suggesting that a narrow growth window is available to achieve layer-by-layer growth of TMDs with adjustable thickness.[82–84] While experimental reports continue to be published rapidly, theoretical modeling has been behind and has not provided significant *a priori* guidance for optimizing the CVD or MOCVD processes. For example, instead of the growth of (Mo, W) (S, Se)$_2$ in the equilibrium 2H crystal structure, it appears to grow in stacked multiple 1H-structured layers. When TMD growth is performed under TM-rich conditions (i.e., chalcogen-poor conditions), TM-rich nuclei form in 3D clusters and multiple layers of TMDs grow laterally, resulting in stacked 1H-structured layers and preventing accurate thickness control [Fig. 3(b)].[82] Under very chalcogen-rich growth environments (i.e., very TM-poor conditions), two chalcogen-terminated edges in close proximity to each other can appear as a line of metal vacancies, which can initiate screw dislocation.[83,84] Screw dislocations can break the symmetry of the crystal structure and promote spiral TMD island formation with various stacking behaviors [Fig. 3(c)]. The growth from these chalcogen-terminated edges generates multiple layers of triangular TMD islands that lack inversion symmetry. In layered crystals, different edge geometries, such as armchair and zigzag, can exhibit different reactivities and growth rates, forming islands of concentric triangles in equilibrium instead of hexagonal grains.[85–87] Therefore,

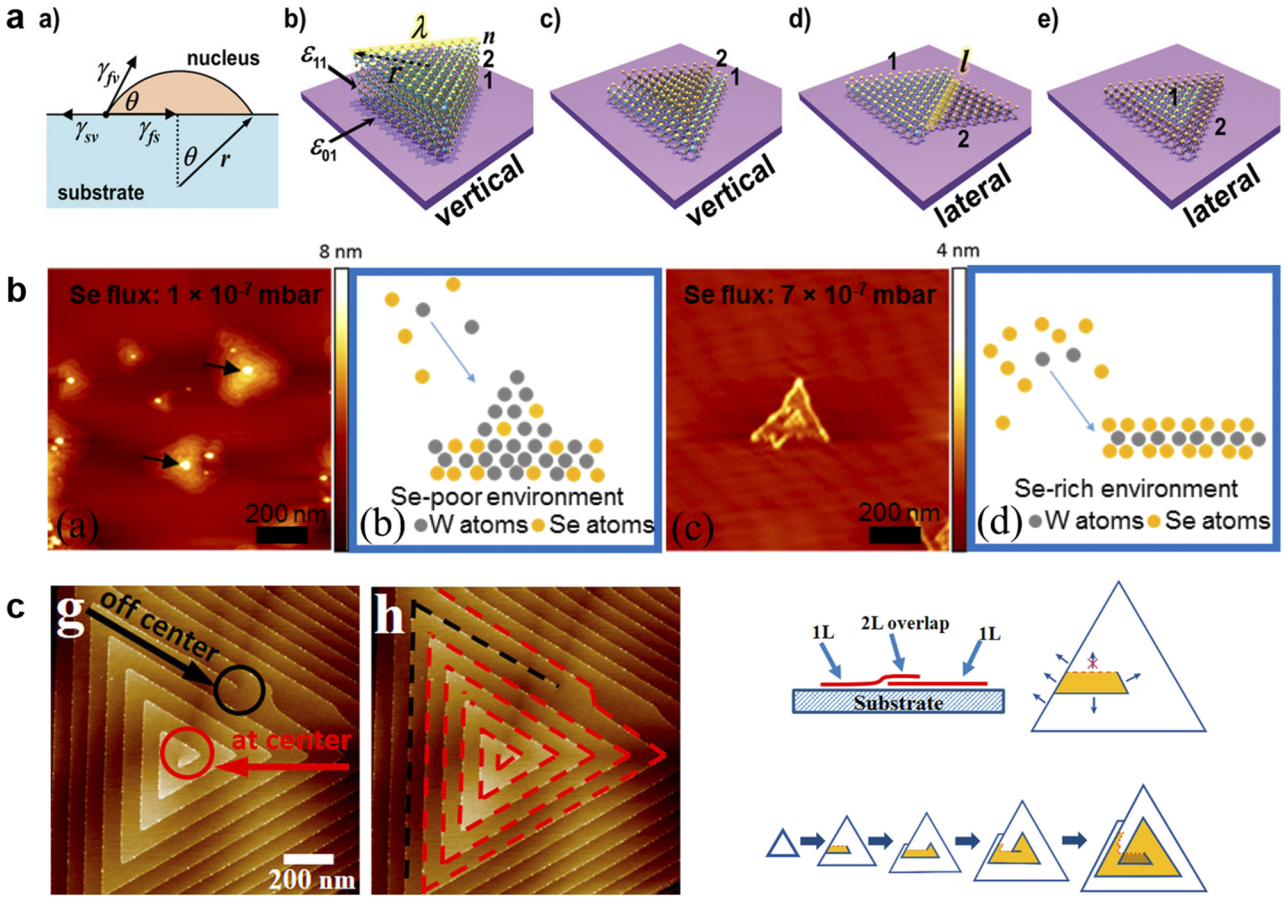

FIG. 3. (a) A revised theory for thin film growth of layered vdW atomic crystals reproduced with permission from Kim *et al.*, Adv. Mater. **31**, 1804939 (2019). Copyright 2019 WILEY-VCH Verlag GmbH & Co. KGaA. (b) Formation of WSe_2 nucleation under W-rich and Se-rich environments, respectively, reproduced with permission from Yue *et al.*, 2D Mater. **4**, 045019 (2017). Copyright 2017 IOP Publishing. (c) Formation of defect-mediated WSe_2 spirals reproduced with permission from Fan *et al.*, Nano Lett. **18**, 3885 (2018). Copyright 2018 American Chemical Society.

the chalcogen (X) to TM (X/TM) ratio must be maintained within a narrow optimum window to enable the layer-by-layer growth of layered TMDs.

Growth conditions and materials purity

The basic growth parameters that are varied during MOCVD include the growth temperature and pressure, mass flow rates, precursor ratios, and substrate tilt/rotation. For the MOCVD growth of TMDs, temperatures ranging from ~550 °C to ~1000 °C have been used, with the relatively low melting temperature materials, including MoS_2, generally grown at the lower end of that range and high melting temperature materials, such as WSe_2, grown at the higher end of that range.[36–46,70–77] Recently, MOCVD systems have been operated at reduced pressures for TMD growth in the range of ~5 Torr to 200 Torr because low-pressure operation facilitates the simultaneous achievement of good uniformity over large areas and abrupt interfaces in the growing films. Almost all of TMD growth is performed using X/TM ratios between 100 and 10 000 with MoS_2 and WSe_2 as representative examples. This is because the addition of high vapor pressure group 6 species in excess of the stoichiometric concentration is rejected back into the vapor during growth. Large areas of TMD were also grown by Eichfeld *et al.*, showing that the growth temperature and pressure, mass flow rates, and precursor ratios affect the quality of the layers grown.[42] A major breakthrough for TMD materials is the establishment of robust *n* and *p* dopants as TMDs present challenges in terms of growth conditions and source chemistry.

Based on the classical Grove's model,[7,50] it is expected that the TMD growth rate would be largely independent of the substrate temperature, proportional to the inlet TM molar flow rate, and independent of the inlet group 6 molar flow rate over a wide temperature range. This is consistent with a growth regime wherein the growth rate is limited by the gas phase diffusion of TM species through the boundary layer above the substrate. As described in the section titled Growth modes, the input X/TM ratio must be maintained within a narrow window to achieve layer-by-layer 2D growth in the layered TMD crystals.

Unintentional carbon and oxygen incorporation should be prevented during the preparation of MOCVD-grown films.[47–50] Carbon generally originates from the MO sources, but the purity of the most widely used MO compounds is consistently good. Oxygen is generally incorporated from atmospheric contamination, but can be minimized by careful attention to the integrity of the MOCVD reactor and using gettering techniques. Both carbon and oxygen contamination can be further reduced by using alternative source chemistries from suppliers. Regarding hydride sources, the major impurity is often the relatively large and highly variable amounts of H_2O (several tens of ppm). In terms of electrically active species formation, most efforts dedicated toward improving purity have focused on reducing metallic impurities in the source materials.

CURRENT STATUS AND CHALLENGES

MOCVD has the potential to realize the wafer-scale growth of single-crystal-like 2D TMD materials on various semiconducting or insulating substrates in a reproducible manner; however, a number of long-standing processing and technological issues impede its practical use. For the sake of simplicity, we will focus our attention on MoS_2 and WSe_2 in the discussions below.

Limited grain sizes

A prerequisite for the deployment of 2D TMD materials in electronic and optoelectronic applications is the ability to mass-produce them while ensuring satisfactory crystal quality and performance. The current challenge with growing MoS_2 and WSe_2 under typical growth conditions is that it results in many small grains (generally sized less than 1 μm), which can limit the performances of devices fabricated from these films. Figures 4(a) and 4(b) shows average grain sizes and lateral growth rates based on the growth temperature for previously reported MoS_2 and WSe_2 grown by MOCVD, respectively. In general, a higher growth temperature generates a larger grain size in the MoS_2 film because of reduced nucleation density.[39,71] However, chalcogen adatoms desorb at much higher rates than do TM adatoms at a given temperature, and this phenomenon is even more severe at the elevated growth temperatures, forcing the introduction of very chalcogen-rich growth environments. Moreover, a high growth temperature process usually causes the retarded growth rates, leading to a low yield. For example, the MOCVD growth of wafer-scale MoS_2 generally took several hours or even a whole day.[36] In addition to the growth temperature, substrate pretreatment is another factor that increases the grain size. Andrzejewsk *et al.* expect that pre-annealing under H_2 could decrease nucleation density and improve surface roughness.[74] MoS_2 grown using pre-annealed sapphire under H_2 produces a grain that is twice the size as that of other samples, as shown in Fig. 5(a). Similar to the mechanism proposed by Simonson *et al.*, they confirmed that the grain size of MoS_2 grown on Gorilla glass (GG) increases with the increase in growth temperature from 400 °C to 600 °C and the power of the plasma treatment (0–40 W) using N_2.[71] As a result, they achieved a domain size of MoS_2 (~32 nm) on plasma-treated GG at 600 °C, which was greater than that on sapphire (~18 nm). However, these factors slightly affect the larger grain size of MoS_2, which is still quite small at less than 1 μm. Kim *et al.* showed that the effect of the S/Mo ratio on the grain size is very low.[77]

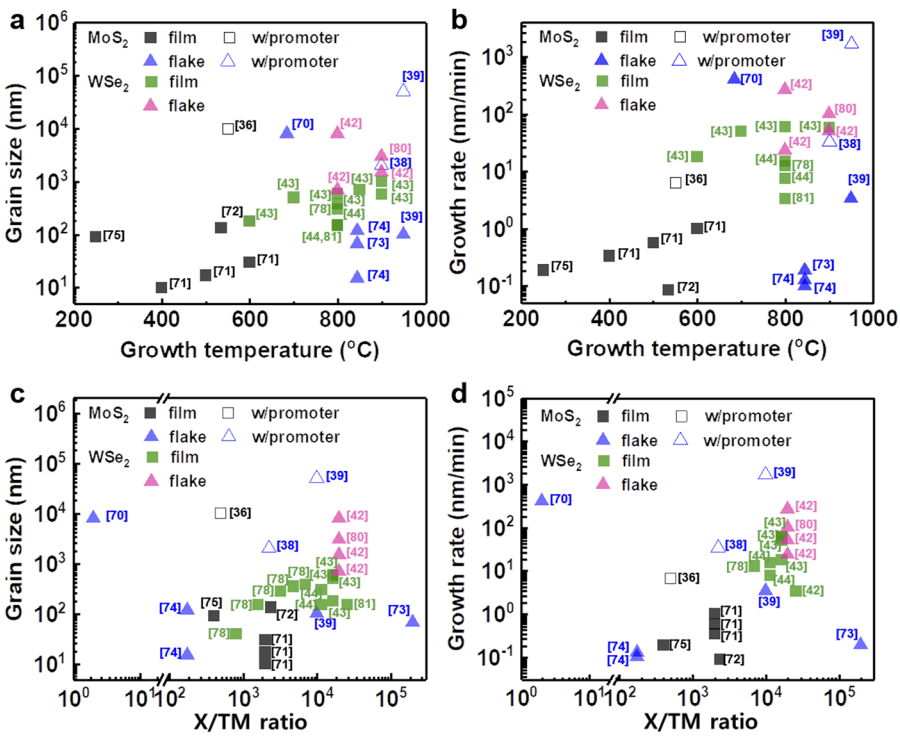

FIG. 4. (a) Grain size and (b) growth rate of MOCVD-grown MoS_2 and WSe_2 as a function of growth temperature. (c) Grain size and (d) growth rate of MOCVD-grown MoS_2 and WSe_2 as a function of flux ratio of chalcogen (X) to transition metal (TM) precursors.

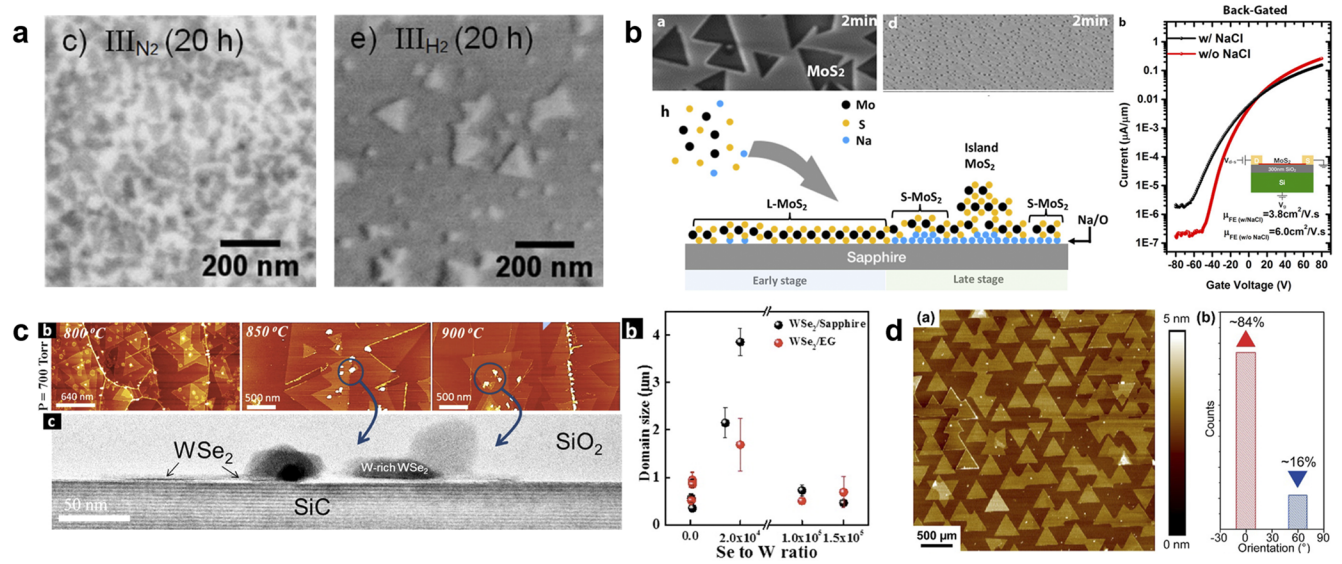

FIG. 5. (a) Effect of substrate treatment on MoS_2 growth reproduced with permission from Andrzejewski *et al.*, Nanotechnology **29**, 295704 (2018). Copyright 2018 Springer Nature. (b) Effect of growth promoter (e.g., NaCl and KI) on MoS_2 growth reproduced with permission from Zhang *et al.*, ACS Appl. Mater. Interfaces **10**, 40831 (2018). Copyright 2018 American Chemical Society. (c) Effect of growth temperature and Se/W ratio on WSe_2 growth reproduced with permission from Eichfeld *et al.*, ACS Nano **9**, 2080 (2015). Copyright 2015 American Chemical Society. (d) Highly oriented WSe_2 epitaxial growth on a defect-controlled h-BN substrate reproduced with permission from Zhang *et al.*, ACS Nano **13**, 3341 (2019). Copyright 2018 American Chemical Society.

Recently, to increase the grain size to more than hundreds of micrometers, Kang *et al.* employed alkali metal halides such as KI and NaCl to reduce the concentration of water and suppress the nucleation in the MOCVD system.[36] Their role was demonstrated by Kim *et al.* in which the growth processes were compared in the absence of KI and NaCl, resulting in an increased growth rate.[39] The researchers performed a pre-exposure of the sapphire substrate to $Mo(CO)_6$ with a very tiny amount of KI prior to the growth stage. They achieved a boosted domain size of MoS_2 (>10 μm) of more than two orders of magnitude as compared to the one-growth-step approach. As another example, Zhang *et al.* confirmed that NaCl-assisted growth induced the substrate surface saturated with Na–O bonds, as shown in Fig. 5(b).[38] Thus, MoS_2 nucleates and grows on top of the Na–O layer, which enhances Mo and S adatom mobilities. As a result, NaCl-assisted MoS_2 has a domain size of at least 1 μm as compared to the grown MoS_2 without NaCl (≈50 nm). Although the carrier mobility can be significantly improved by increasing the grain size in polycrystalline MoS_2 samples due to defect scattering,[88] the NaCl-assisted grown MoS_2 film degrades the device performance because the Na–O interface that forms during the growth suppresses the charge transfer from the substrate.

Like MoS_2, a higher growth temperature usually leads to a larger grain size in WSe_2 growth. Eichfeld *et al.* initially succeeded in generating uniform WSe_2 thin film growth on sapphire through MOCVD using tungsten hydrocarbonyl and dimethylselenium. However, the MOCVD-grown WSe_2 samples were nanocrystalline.[41] In their follow-up research, scalable WSe_2 flakes of up to ~8 μm were successfully grown using the MOCVD method as the growth temperature increased from 600 to 900 °C.[42] Moreover, as shown in the TEM image of Fig. 5(c), at constant total pressure and growth temperature, a low Se:W ratio (≈100) induced the formation of 3D nuclei clusters, which occur under TM-rich conditions. As the Se:W flux ratio increased to 20 000, the domain size of the WSe_2 flakes also increased due to the reduction in the nucleation density and the number of Se vacancies [Figs. 4(c) and 4(d)]. Above a Se:W flux ratio of 20 000, however, the domain size begins to decrease again due to Se vapor saturation. In addition to the growth temperature and Se:W flux ratio, Zhang *et al.* confirmed large-area coalesced WSe_2 monolayer epitaxial growth on sapphire through a multistep diffusion-mediated process consisting of nucleation, ripening, and lateral growth steps.[43] After the nucleation steps, the supply of tungsten hydrocarbonyl, which is a W precursor, was stopped, resulting in an increase in domain size and a decrease in cluster density. This was followed by the ripening step. Then, during the lateral growth step, low tungsten hydrocarbonyl flow increased only the lateral domain size, leading to a fully coalesced WSe_2 monolayer. In addition, to prevent the formation of amorphous carbon layers and improve the crystal quality, the Se precursor source of dimethyl selenium was changed to hydrogen selenide.[78] Furthermore, Zhang *et al.* confirmed that nucleation and orientation of WSe_2 flakes on h-BN could be controlled by controlling h-BN defects in Fig. 5(d).[44] They controlled the h-BN defect sites through annealing in NH_3 at 1100 °C for 30 min. As a result, the WSe_2 triangular domains grew epitaxially on the h-BN surface with only two orientations in the majority of the domains (≈84%).

Grain-size-dependent-mobilities

As summarized in Fig. 6, a higher field effect mobility (μ_{FE}) above 10 cm^2 V^{-1} s^{-1} at RT could be observed in the devices with

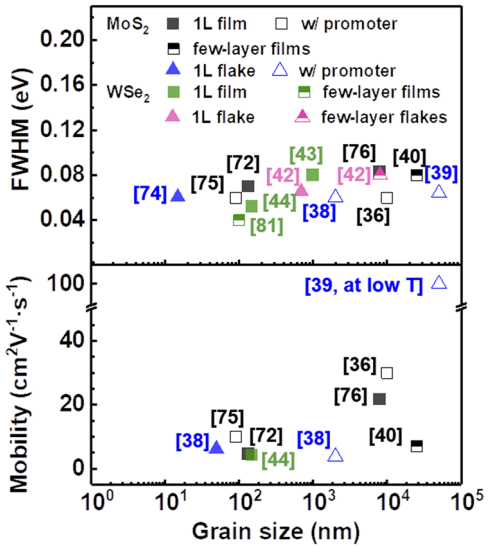

FIG. 6. Mobility and PL FWHM of MoS_2 and WSe_2 as a function of grain size.

relatively large grain sizes (>5 μm). It is found that the value of μ_{FE} increases with the grain size. In particular, even higher μ_{FE} of ~30 $cm^2\ V^{-1}\ s^{-1}$ was shown for a monolayer MoS_2 film with high crystalline quality [~0.06 eV, full width at half maximum (FWHM) of the photoluminescence (PL) spectrum] via MOCVD.[36] However, the value of μ_{FE} for a previously reported MOCVD-grown MoS_2 film is still lower than ~410 $cm^2\ V^{-1}\ s^{-1}$ based on the first principles calculations,[89] although PL peaks for MoS_2 display low values for FWHM, similar to that of a mechanically exfoliated MoS_2 flake (~0.06 eV).[90] In the case of WSe_2, even though in the early stage of MOCVD growth, the mobility of the MOCVD-grown bilayer WSe_2 film exhibited ~30 $cm^2\ V^{-1}\ s^{-1}$, which is comparable to the high-quality CVD-grown WSe_2 samples.[79] The extracted FWHM of the PL peak with different grain sizes of MoS_2 and WSe_2 also illustrates, in this case of no drastic difference in the grain size, crystallinity to be one of the major reasons. Kumar *et al.* reported μ_{EF} values obtained from MoS_2 of a different number of layers and estimated μ_{EF} of ~7.1 $cm^2\ V^{-1}\ s^{-1}$ in the top-gate configuration for trilayer MoS_2 films with on–off ratios of ~10^5.[40] This is in contrast to the reported literature results, indicating that thicker MoS_2 transistors exhibit higher mobilities.[9,91] They speculated that mobility degradation originates from defect scattering because large FWHM of the in-plane phonon mode (E^1_{2g}) from the Raman spectrum was obtained, indicating poor crystallinity.

In addition, various factors including the device structure, dielectric layer, and roughness at the interface play a major role in FET characteristics. As mentioned in the section titled Limited Grain Sizes, although the grain size (~2 μm) of a grown monolayer MoS_2 flake ($MoS_{2(NaCl)}$) via NaCl-assisted growth is approximately two orders of magnitude larger than that of the grown monolayer MoS_2 flake without NaCl, μ_{EF} of $MoS_{2(NaCl)}$ is degraded by >30% compared to that of MoS_2 due to the formation of a byproduct (Na–O) at the interface between the substrate and channel.[38] Zhang *et al.* proved that the improved hole μ_{FE} of ~4.2 $cm^2\ V^{-1}\ s^{-1}$ extracted from the device fabricated using WSe_2 epitaxially grown on h-BN was higher than the electron μ_{FE} of WSe_2 grown on sapphire (~0.3 $cm^2\ V^{-1}\ s^{-1}$).[44] It is consistent with previously reported results that h-BN improves mobility and reduces the interface states.[92,93] Therefore, the large-scale synthesis of TMD films with low concentration of defects and byproducts by controlling the growth on the desired substrate through MOCVD remains a challenge for practical application.

Defect engineering

2D TMD materials are, by definition, entirely surface materials; hence, their electronic and optoelectronic properties are fatally affected by material disorder. During the MOCVD growth of TMDs, structural defects are inevitably introduced, and immense effort has to be expended to achieve the required levels of high quality. Structural defects, including vacancies, interstitials, and GBs, can modify the electrical and optical properties of TMDs for targeted applications.[7] While the electronic and optoelectronic performance of TMD-based devices can be improved with the reduction of external disorder arising from the environment, the issue of intrinsic material quality should be addressed to achieve significant progress in the field.

Based on theoretical calculations in both the monolayer and bulk of MoS_2 (see Table II),[94–101] a mono-sulfur (S) vacancy (V_S) and a single S interstitial (S_I) are found to have low formation energy under Mo-rich and S-rich conditions, respectively. These results are consistent with experimental results, indicating that V_S is frequently observed in mechanical exfoliated[102] and grown samples[95,103] using STM [Fig. 7(a)]. Most MoS_2 with Vs exhibit *n*-type behavior,[103,104] whereas a mono-molybdenum (Mo) vacancy (V_{Mo}) in MoS_2 induces *p*-type characteristics.[40] In addition, V_S sites strongly trigger the adsorption of molecules such as CO_2, N_2, and H_2O because of a low adsorption energy when the defective MoS_2 with Vs is exposed to ambient air,[105,106] as shown in Table III. Nan *et al.* reported that the passivation of Vs in MoS_2 exhibited the *p*-type behavior induced by oxygen chemical adsorption in Vs.[107] Although the origin of *n*-type behavior is unclear, electrical behavior is determined based on the concentration of unintentionally doped vacancies (i.e., V_S, V_{2S}, and V_{Mo}) in MoS_2. More importantly, in the synthesized polycrystalline MoS_2, the S vacancy concentration relies on more than just the defect formation energy (E_f), as (4|6) defect complexes (V_{2s} and Mo_I) are induced by the (5|7) defects at S-polar GBs during growth at relatively high temperatures, as shown in Figs. 7(b) and 7(c).[99] These defect complexes are easily formed when polycrystalline MoS_2 is synthesized at a higher temperature or with a smaller grain size and in a high-angle grain boundary (GB), indicating that control of S vacancy concentration can be achieved by growth parameters, including growth temperature, growth time, and ratio of molecular gases.

Based on theoretical calculations, in the monolayer of WSe_2 (Table II),[97,100,108–113] the selenium vacancy (V_{Se}) is energetically favorable under S-rich conditions and creates deep acceptor states that result in efficient electron traps and deteriorates the carrier mobility. These results are consistent with experimental results, indicating that V_{Se} is frequently observed in CVD-grown WSe_2 samples while tungsten vacancy (V_W) is not present, and when using STM.[109] Like MoS_2, V_{Se} in WSe_2 act as donor sites, resulting in

TABLE II. Defect formation energy for MoS_2 and WSe_2.

Material	Condition		Defect	Formation energy		References
	Thickness	Environment		S-rich	Mo-rich	
MoS_2	Bulk	Vacuum	V_{Mo}	4.7	7.24	94
				4.88	7.67	95
			V_S	2.9	1.66	94
				2.89	1.33	95
			V_{2S}	5.9	2.89	95
			Mo_S	3.42	3.41	94
			S_{Mo}	3.48	7.26	94
			Mo_I	6	3.73	94
			S_I	2.79	4.61	94
	Monolayer	Vacuum	V_{Mo}	4.85	7.27	94
				4.38	7.04	96 and 97
				4.61	7.24	98 and 99
			V_{Mo} in GB	0.6	3.16	10
			V_S	2.85	1.56	94
				2.52	1.5	96 and 99
				2.66	1.33	97, 98, and 100
				2.35	0.95	101
			V_S in GB	0.27	−1	99
			V_{2S}	5.28	2.63	97 and 98
				5.37	2.61	99
			V_{2S} in GB	1	−1.5	99
			Mo_S	4.17	4.2	94
				7.7	4.61	98
			S_{Mo}	4.85	8.03	94
				4.53	8	98
			Mo_I	6	3.58	94
				7.2	4.3	96
				6.52	4.32	99
			Mo_I in GB	0.68	−1.82	99
			S_I	0.9	2.14	94 and 96
				1.14	2.5	99
			S_I in GB	−0.86	1.12	99
WSe_2			V_{Mo}	3.35	6.48	97
				3.51	...	108
				3.85	5.07	109
				3.95	...	110
			V_{Se}	2.68	...	108
				2.69	...	100
				2.71	1.58	97 and 110
				2.8	2.2	109
				2.81	...	111

TABLE II. (*Continued.*)

Material	Condition		Defect	Formation energy		References
	Thickness	Environment		S-rich	Mo-rich	
WSe_2	Monolayer	Vacuum	V_{2Se}	4.89	...	112
				4.93	2.96	97
				5.03	3.8	109
			W_{Se}	3.65	5.51	109
			Se_W	3.32	...	110
			W_I	4.6	5.8	109
				7.35	5.63	97
			Se_I	1.38	2.24	97
				3.2	3.8	109

n-type doping, whereas V_W in WSe_2 induce *p*-type doping. Tosun *et al.* found that WSe_2 can induce air-stable *n*-type doping by H_2 plasma-induced anion vacancy formation.[114] However, WSe_2 is also susceptible to unintended chemical interactions with the environment. Recently, Ma *et al.* found that an O-doped WSe_2 monolayer through NO chemisorption could completely remove the defect levels from the V_{Se}.[113] Defect formation and chemical interactions with gas molecules in TMD layers considerably influence the electrical properties of TMDs.[29,115,116] Therefore, defect engineering is a crucial step in the use in suitable applications.

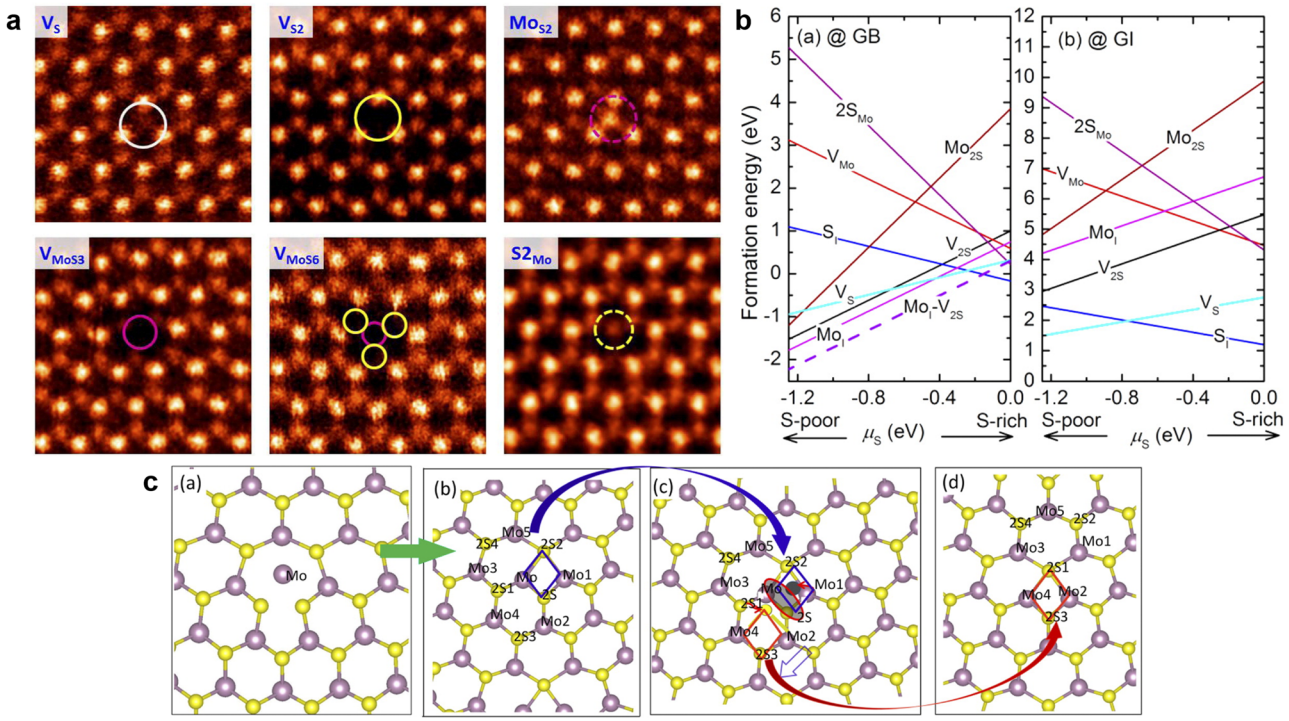

FIG. 7. Intrinsic point defects in MoS_2. (a) Atomic-resolution annular dark field (ADF) images of different types of intrinsic point defects in the CVD-grown MoS_2 monolayer reproduced with permission from Zhou *et al.*, Nano Lett. **13**, 2615 (2013). Copyright 2013, American Chemical Society. (b) Formation energies of various point defects at the grain boundary (GB) and grain interior (GI) of the polycrystalline MoS_2 monolayer as a function of sulfur chemical potential (μ_S). (c) Schematic of the formation of (4|6) defect complexes from (5|7) defects at S-polar GBs induced by high growth temperatures reproduced with permission from Yu *et al.*, Nano Lett. **15**, 6855 (2015). Copyright 2015 American Chemical Society.

TABLE III. Adsorption energy at S vacancy (V_S and Se vacancy (V_{Se}) in MoS_2 and WSe_2.

Material	Condition		Adsorption in S vacancy		Formation energy	References
	Thickness	Environment				
MoS_2	Monolayer	Vacuum	Physisorption	CO_2	0.17	105
				N_2	0.114	105
				H_2O	0.234	105
				CO	0.19	106
				NO	0.23	106
				NO_2	0.31	106
			Chemisorption	CO	1.163	106
					1.21	106
				NO	2.642	105
					2.81	106
				O_2	2.092	98
					1.843	100
					1.822	105
				NH_3	0.407	105
WSe_2	Monolayer	Vacuum	Physisorption	O_2	0.24	112
				H_2O	0.3	113
				N_2	0.17	113
				CO	0.23	113
				NO	0.37	113
				NO_2	0.36	113
				N_2O	0.24	113
			Chemisorption	O_2	1.6	109
					2.43	100
				N_2	−0.08	113
				CO	1.57	113
				NO	3.15	113

Doping engineering

Most advances in 3D semiconductor devices rely on the availability and subsequent doping of high purity materials. The doping of two or more synthesized TMD layers is critical in tuning electrical, optical, and magnetic properties, including conductivity and charge density.[90,117–132] Table IV lists the primary strategies used in doping engineering, including the charge transfer and atomic substitution. As previously mentioned, the presence of Vs in MoS_2 enables the formation of substitutional dopants at the Vs sites. Dolui *et al.* proved that doping of halogens at Vs produces more stable thermodynamic conditions.[121] Chuang *et al.* found that Nb doping on MoS_2 and WSe_2 can reduce the contact resistance to metal electrodes, and introducing a Nb-doped WSe_2 layer between as-grown WSe_2 and a metal electrode can improve the mobilities of all FETs.[130] More specifically, excellent mobilities of ~180 cm^2 V^{-1} s^{-1} and ~220 cm^2 V^{-1} s^{-1} for MoS_2- and WSe_2-based FETs, respectively, were observed. However, this method can destroy the structure of FETs because dopant atoms are incorporated into the lattice.[122] In the case of surface charge transfer doping, host materials avoid unintended lattice distortion and damage. Choi *et al.* fabricated a *p–n* junction using the doping chemical benzyl viologen as an *n*-type dopant and $AuCl_3$ as a *p*-type dopant on MoS_2 layers.[119] The fabricated device showed a highly efficient photoresponse and ideal rectifying behavior induced by the formation of a *p–n* junction. Zhao *et al.* confirmed that *p*-type degenerate doping of NO_2 gas to WSe_2 can enhance carrier concentration by up to $\approx 10^{19}$ cm^{-3} through NO_2 surface treatment at 150 °C, resulting in NO_2 chemisorption on the V_{Se} of WSe_2.[126] When the NO_2 chemisorption strategy was applied to WSe_2 channel edges and contacted with Pd/Au electrodes, the contact resistance between WSe_2 and the electrodes were considerably reduced from ~0.13 GΩ μm to ~1.27 kΩ·μm, resulting in a high effective hole mobility of ~250 cm^2 V^{-1} s^{-1} and a sub-threshold swing of ~60 mV/dec.[9] This is a field of intense study that should be significantly investigated in the coming years.

TABLE IV. Doping strategy for MoS_2 and WSe_2.

	Dopant	Type	Doping strategy	Carrier concentration (cm^{-2})	Mobility ($cm^2\ V^{-2}\ s^{-1}$)	Application with doped MX_2	References
MoS_2	Benzyl viologen (BV)	n	Charge transfer (wet chemical)	1.2×10^{13} ... 2.9×10^{13}	24.7 ... 44	Top-gate FET p–n FET (back-gate) p–n FET (back-gate)	117 118 119
	$AuCl_3$	p	Charge transfer (wet chemical)	... 2.4×10^{8}	... 13	p–n FET (back-gate) p–n FET (back-gate)	118 119
	APTES	n	Charge transfer (wet chemical)	1.0×10^{11}	142.2	Photodetector	120
	NH^{4+} BF^{4-}	n p	Charge transfer (ionic liquids)	... ...	... ...	Metal–superconductor metal–insulator and transistor	121
	Nb	p	Substitutional doping (thermal annealing by CVT)	2.8×10^{14}	14	FET	122
	Fe	n	Substitutional doping (thermal annealing by CVT)	1.1×10^{13}	49	...	123
	Re	n	Substitutional doping (thermal annealing by CVD)	5.5×10^{12}	...	FET	124
	F4-TCNQ	p	Charge transfer (self-assembled monolayer)	...	...	FET	90
	H N	n p	DFT simulation (dry nonmetal doped)	... ...	... ...	...	125
	Fe, Cl, B, I	n	DFT simulation (dry doping)	...	...	...	121
WSe_2	NO_2	p	Charge transfer (gaseous molecules)	2.2×10^{12} 4.38×10^{16} (bulk, cm^{-3})	250	FET	9 126
	OTS	p	Charge transfer (self-assembled monolayer)	1.4×10^{11}	168.8	FET and photodetector	120
	K	n	Charge transfer (thermal evaporation)	2.5×10^{12}	110	FET	127
	F4-TCNQ	p	Charge transfer (self-assembled monolayer)	...	42.6	p–n FET	128
	S	n	Substitutional doping (thermal annealing by CVD)	...	68.2	FET	129
	Nb Re	p n	Substitutional doping (thermal annealing by CVT)	... ...	220 at RT 2100 at 5 K ...	FET	130

TABLE IV. (*Continued*.)

Dopant	Type	Doping strategy	Carrier concentration (cm^{-2})	Mobility ($cm^2\ V^{-2}\ s^{-1}$)	Application with doped MX_2	References
Nb	p	Substitutional doping (thermal annealing by CVT)	...	150 at RT 300 at 80 K	Photodetector	131
Te	p	Substitutional doping (thermal annealing by CVT)	...	46	FET	132

OUTLOOK

We conclude by noting that research on 2D TMD atomic sheets began only a few years ago, with the first papers on mechanically exfoliated[8] and CVD-grown[133] MoS_2 FETs being published in 2011 and 2012, respectively. The critical issues restricting the widespread implementation of these 2D vdW materials into high-performance devices remain to be addressed. GB formation must be significantly mitigated to obtain single-crystal-like 2D TMD films for efficient charge carrier transport.[7] Digital thickness control and lateral/vertical growth of TMD heterostructures have yet to be truly demonstrated in a reproducible manner. Defect and doping control is only in its infancy, and continuous improvement in encapsulation and device fabrication techniques needs to be further explored. Therefore, the path to commercialization is not exactly predictable. However, the progress of a technology from its discovery to its realization as a commercial product is generally very slow and meandering. We believe that sustained worldwide effort addressing the major challenges will be inevitable toward realizing the potential of 2D TMD materials in practical high-performance electronic and optoelectronic devices, as already demonstrated with exfoliated flakes from bulk crystals shown in Table I. While devices fabricated from synthesized TMD films by MOCVD (also by MBE) are only in their infancy, the versatile MOCVD technique will provide a new avenue for the growth and integration of different high-quality, multi-dimensional TMD films with different compositions and physical properties on a single substrate, thereby enhancing batch fabrication and further development of atomically thin integrated circuitry. As witnessed by the success of Si and III–V (or II–VI) compound semiconductor technologies, more rigorous device specifications and increased device complexity, coupled with the excellent uniformity, continue to drive the need for improved thickness, composition, and doping uniformity over large areas in this rapidly emerging field.

Parallelly, much effort is needed to improve the quality of 2D vdW materials that can be grown by MOCVD while maintaining and improving the inter- and intra-wafer uniformity on increasingly large substrates for real commercialization. This effort will also be aided by notable improvements in MOCVD equipment design and construction, particularly on the part of equipment vendors. Simultaneous achievement of three attributes (i.e., large-scale growth, interfacial abruptness, and uniformity) will be necessary for diverse device applications. Up to date, there has been almost no demonstration of all three attributes in the same apparatus.[7] Likely approaches to improve uniformity include supplying continuous and uniform atomic source species using a run/vent manifold system and modifying the hydrodynamics and thermal geometry of the reactor with rotating disk technology to obtain a uniform boundary layer thickness and thereby uniform incorporation/evaporation rates of species from the surfaces.[50] For economic viability, a greater understanding of hydrodynamics and thermal geometry of the reactor, consensus on the design of MOCVD systems, particularly reaction chambers, and a future market that demands excellence will be highly required.

AUTHOR'S CONTRIBUTIONS

D.H.L. and Y.S. contributed equally to this work.

ACKNOWLEDGMENTS

This work was supported by the Research Fund (Grant No. 1.190093.01) of UNIST, the Basic Science Research Program (Grant Nos. 2017R1E1A1A01075283 and 2019M2D2A1A02059152), and the Nano·Material Technology Development Program (Grant No. 2017M3A7B8065377) through the National Research Foundation (NRF) of Korea funded by the Ministry of Science, ICT, and Future Planning.

REFERENCES

[1] A. K. Geim and I. V. Grigorieva, Nature **499**, 419 (2013).
[2] Y. Liu, P. Stradins, and S.-H. Wei, Sci. Adv. **2**, e1600069 (2016).
[3] X. Li, L. Tao, Z. Chen, H. Fang, X. Li, X. Wang, J.-B. Xu, and H. Zhu, Appl. Phys. Rev. **4**, 021306 (2017).
[4] J. A. Robinson, APL Mater. **6**, 058202 (2018).
[5] Z. Lin, Y. Lei, S. Subramanian, N. Briggs, Y. Wang, C.-L. Lo, E. Yalon, D. Lloyd, S. Wu, K. Koski, R. Clark, S. Das, R. M. Wallace, T. Kuech, J. S. Bunch, X. Li, Z. Chen, E. Pop, V. H. Crespi, J. A. Robinson, and M. Terrones, APL Mater. **6**, 080701 (2018).
[6] X. Lin, W. Yang, K. L. Wang, and W. Zhao, Nat. Electron. **2**, 274 (2019).
[7] S.-Y. Kim, J. Kwak, C. V. Ciobanu, and S.-Y. Kwon, Adv. Mater. **31**, 1804939 (2019).
[8] B. Radisavljevic, A. Radenovic, J. Brivio, V. Giacometti, and A. Kis, Nat. Nanotechnol. **6**, 147 (2011).
[9] H. Fang, S. Chuang, T. C. Chang, K. Takei, T. Takahashi, and A. Javey, Nano Lett. **12**, 3788 (2012).

[10]Q. A. Vu, Y. S. Shin, Y. R. Kim, W. T. Kang, H. Kim, D. H. Luong, I. M. Lee, K. Lee, D.-S. Ko, J. Heo, S. Park, Y. H. Lee, and W. J. Yu, Nat. Commun. **7**, 12725 (2016).
[11]C. Liu, X. Yan, X. Song, S. Ding, D. W. Zhang, and P. Zhou, Nat. Nanotechnol. **13**, 404 (2018).
[12]O. Lopez-Sanchez, D. Lembke, M. Kayci, A. Radenovic, and A. Kis, Nat. Nanotechnol. **8**, 497 (2013).
[13]W. Zhang, M.-H. Chiu, C.-H. Chen, W. Chen, L.-J. Li, and A. T. S. Wee, ACS Nano **8**, 8653 (2014).
[14]W. J. Yu, Y. Liu, H. Zhou, A. Yin, Z. Li, Y. Huang, and X. Duan, Nat. Nanotechnol. **8**, 952 (2013).
[15]B. W. Baugher, H. O. Churchill, Y. Yang, and P. Jarillo-Herrero, Nat. Nanotechnol. **9**, 262 (2014).
[16]C.-H. Lee, G.-H. Lee, A. M. van der Zande, W. Chen, Y. Li, M. Han, X. Cui, G. Arefe, C. Nuckolls, T. F. Heinz, J. Guo, J. Hone, and P. Kim, Nat. Nanotechnol. **9**, 676 (2014).
[17]F. Withers, O. Del Pozo-Zamudio, A. Mishchenko, A. P. Rooney, A. Gholinia, K. Watanabe, T. Taniguchi, S. J. Haigh, A. K. Geim, A. I. Tartakovskii, and K. S. Novoselov, Nat. Mater. **14**, 301 (2015).
[18]J. S. Ross, P. Klement, A. M. Jones, N. J. Ghimire, J. Yan, D. Mandrus, T. Taniguchi, K. Watanabe, K. Kitamura, W. Yao, D. H. Cobden, and X. Xu, Nat. Nanotechnol. **9**, 268 (2014).
[19]M. M. Furchi, A. Pospischil, F. Libisch, J. Burgdörfer, and T. Mueller, Nano Lett. **14**, 4785 (2014).
[20]A. Ramasubramaniam, Phys. Rev. B **86**, 115409 (2012).
[21]T. C. Berkelbach, M. S. Hybertsen, and D. R. Reichman, Phys. Rev. B **88**, 045318 (2013).
[22]A. Koma, K. Sunouchi, and T. Miyajima, Microelectron. Eng. **2**, 129 (1984).
[23]A. Koma and K. Yoshimura, Surf. Sci. **174**, 556 (1986).
[24]K. Saiki, K. Ueno, T. Shimada, and A. Koma, J. Cryst. Growth **95**, 603 (1989).
[25]K. Ueno, T. Shimada, K. Saiki, and A. Koma, Appl. Phys. Lett. **56**, 327 (1990).
[26]K.-K. Liu, W. Zhang, Y.-H. Lee, Y.-C. Lin, M.-T. Chang, C.-Y. Su, C.-S. Chang, H. Li, Y. Shi, H. Zhang, C.-S. Lai, and L.-J. Li, Nano Lett. **12**, 1538 (2012).
[27]A. Tarasov, P. M. Campbell, M. Y. Tsai, Z. R. Hesabi, J. Feirer, S. Graham, W. J. Ready, and E. M. Vogel, Adv. Funct. Mater. **24**, 6389 (2014).
[28]K.-A. N. Duerloo, Y. Li, and E. J. Reed, Nat. Commun. **5**, 4214 (2014).
[29]S.-Y. Kim, J. Kwak, J. H. Kim, J.-U. Lee, Y. Jo, S. Y. Kim, H. Cheong, Z. Lee, and S.-Y. Kwon, 2D Mater. **4**, 011007 (2017).
[30]S. V. Mandyam, M.-Q. Zhao, P. M. Das, Q. Zhang, C. C. Price, Z. Gao, V. B. Shenoy, M. Drndic, and A. T. C. Johnson, ACS Nano **13**, 10490 (2019).
[31]Z. Zhang, P. Chen, X. Duan, K. Zang, J. Luo, and X. Duan, Science **357**, 788 (2017).
[32]P. K. Sahoo, S. Memaran, Y. Xin, L. Balicas, and H. R. Gutierrez, Nature **553**, 63 (2018).
[33]P. K. Sahoo, H. Zong, J. Liu, W. Xue, X. Lai, H. R. Gutierrez, and D. V. Voronine, Opt. Mater. Express **9**, 1620 (2019).
[34]M. Ludowise, J. Appl. Phys. **58**, R31 (1985).
[35]G. Stringfellow, *OMVPE, Theory and Practive* (Academic Press, Boston, 1989).
[36]K. Kang, S. Xie, L. Huang, Y. Han, P. Y. Huang, K. F. Mak, C.-J. Kim, D. Muller, and J. Park, Nature **520**, 656 (2015).
[37]B. Kalanyan, W. A. Kimes, R. Beams, S. J. Stranick, E. Garratt, I. Kalish, A. V. Davydov, R. K. Kanjolia, and J. E. Maslar, Chem. Mater. **29**, 6279 (2017).
[38]K. Zhang, B. M. Bersch, F. Zhang, N. C. Briggs, S. Subramanian, K. Xu, M. Chubarov, K. Wang, J. O. Lerach, J. M. Redwing, S. K. Fullerton-Shirey, M. Terrones, and J. A. Robinson, ACS Appl. Mater. Interfaces **10**, 40831 (2018).
[39]H. Kim, D. Ovchinnikov, D. Deiana, D. Unuchek, and A. Kis, Nano Lett. **17**, 5056 (2017).
[40]V. K. Kumar, S. Dhar, T. H. Choudhury, S. Shivashankar, and S. Raghavan, Nanoscale **7**, 7802 (2015).
[41]S. M. Eichfeld, C. M. Eichfeld, Y.-C. Lin, L. Hossain, and J. A. Robinson, APL Mater. **2**, 092508 (2014).
[42]S. M. Eichfeld, L. Hossain, Y.-C. Lin, A. F. Piasecki, B. Kupp, A. G. Birdwell, R. A. Burke, N. Lu, X. Peng, J. Li, A. Azcatl, S. McDonnell, R. M. Wallace, M. J. Kim, T. S. Mayer, J. M. Redwing, and J. A. Robinson, ACS Nano **9**, 2080 (2015).
[43]X. Zhang, T. H. Choudhury, M. Chubarov, Y. Xiang, B. Jariwala, F. Zhang, N. Alem, G.-C. Wang, J. A. Robinson, and J. M. Redwing, Nano Lett. **18**, 1049 (2018).
[44]X. Zhang, F. Zhang, Y. Wang, D. S. Schulman, T. Zhang, A. Bansal, N. Alem, S. Das, V. H. Crespi, M. Terrones, and J. M. Redwing, ACS Nano **13**, 3341 (2019).
[45]S. Xie, L. Tu, Y. Han, L. Huang, K. Kang, K. U. Lao, P. Poddar, C. Park, D. A. Muller, R. A. DiStasio, Jr., and J. Park, Science **359**, 1131 (2018).
[46]Y. Kobayashi, S. Yoshida, M. Maruyama, H. Mogi, K. Murase, Y. Maniwa, O. Takeuchi, S. Okada, H. Shigekawa, and Y. Miyata, ACS Nano **13**, 7527 (2019).
[47]J. O. Williams, Angew. Chem., Int. Ed. Engl. **28**, 1110 (1989).
[48]F. Maury, J. Phys. IV **5**, C5 (1995).
[49]A. G. Thompson, Mater. Lett. **30**, 255 (1997).
[50]M. Ohring, *The Materials Science of Thin Films* (Academic Press, San Diego, 1992).
[51]E. Xenogiannopoulou, P. Tsipas, K. Aretouli, D. Tsoutsou, S. Giamini, C. Bazioti, G. Dimitrakopulos, P. Komninou, S. Brems, C. Huyghebaert, I. P. Radu, and A. Dimoulas, Nanoscale **7**, 7896 (2015).
[52]D. Fu, X. Zhao, Y.-Y. Zhang, L. Li, H. Xu, A.-R. Jang, S. I. Yoon, P. Song, S. M. Poh, T. Ren, Z. Ding, W. Fu, T. J. Shin, H. S. Shin, S. T. Pantelides, W. Zhou, and K. P. Loh, J. Am. Chem. Soc. **139**, 9392 (2017).
[53]H. Xu, D. Han, Y. Bao, F. Cheng, Z. Ding, S. J. Tan, and K. P. Loh, Nano Lett. **18**, 5085 (2018).
[54]S. El Kazzi, W. Mortelmans, T. Nuytten, J. Meersschaut, P. Carolan, L. Landeloos, T. Conard, I. Radu, M. Heyns, and C. Merckling, J. Appl. Phys. **123**, 135702 (2018).
[55]H. J. Liu, L. Jiao, L. Xie, F. Yang, J. L. Chen, W. K. Ho, C. L. Gao, J. F. Jia, X. D. Cui, and M. H. Xie, 2D Mater. **2**, 034004 (2015).
[56]M. Nakano, Y. Wang, Y. Kashiwabara, H. Matsuoka, and Y. Iwasa, Nano Lett. **17**, 5595 (2017).
[57]L. K. Tan, B. Liu, J. H. Teng, S. Guo, H. Y. Low, and K. P. Loh, Nanoscale **6**, 10584 (2014).
[58]A. Valdivia, D. J. Tweet, and J. F. Conley, Jr., J. Vac. Sci. Technol., A **34**, 021515 (2016).
[59]K. Park, Y. Kim, J.-G. Song, S. J. Kim, C. W. Lee, G. H. Ryu, Z. Lee, J. Park, and H. Kim, 2D Mater. **3**, 014004 (2016).
[60]R. Browning, N. Kuperman, R. Solanki, V. Kanzyuba, and S. Rouvimov, Semicond. Sci. Technol. **31**, 095002 (2016).
[61]T. Jurca, M. J. Moody, A. Henning, J. D. Emery, B. Wang, J. M. Tan, T. L. Lohr, L. J. Lauhon, and T. J. Marks, Angew. Chem., Int. Ed. **56**, 4991 (2017).
[62]M. L. Shi, L. Chen, T. B. Zhang, J. Xu, H. Zhu, Q. Q. Sun, and D. W. Zhang, Small **13**, 1603157 (2017).
[63]A. Sharma, M. A. Verheijen, L. Wu, S. Karwal, V. Vandalon, H. C. Knoops, R. S. Sundaram, J. P. Hofmann, W. E. Kessels, and A. A. Bol, Nanoscale **10**, 8615 (2018).
[64]G. Stringfellow, J. Cryst. Growth **68**, 111 (1984).
[65]B. Cockyane and P. J. Wright, J. Cryst. Growth **68**, 223 (1984).
[66]A. Koma, K. Saiki, and Y. Sato, Appl. Surf. Sci. **41**, 451 (1990).
[67]X. Liu, I. Balla, H. Bergeron, G. P. Campbell, M. J. Bedzyk, and M. C. Hersam, ACS Nano **10**, 1067 (2015).
[68]J.-K. Choi, J.-H. Huh, S.-D. Kim, D. Moon, D. Yoon, K. Joo, J. Kwak, J. H. Chu, S. Y. Kim, K. Park, Y.-W. Kim, E. Yoon, H. Cheong, and S.-Y. Kwon, Nanotechnology **23**, 435603 (2012).
[69]K. Y. Ko, J.-G. Song, Y. Kim, T. Choi, S. Shin, C. W. Lee, K. Lee, J. Koo, H. Lee, J. Kim, T. Lee, J. Park, and H. Kim, ACS Nano **10**, 9287 (2016).

[70]B. Wang, Z. Islam, K. Zhang, K. Wang, J. Robinson, and A. Haque, Nanotechnology **28**, 365703 (2017).
[71]N. A. Simonson, J. R. Nasr, S. Subramanian, B. Jariwala, R. Zhao, S. Das, and J. A. Robinson, FlatChem **11**, 32 (2018).
[72]G. Jin, C.-S. Lee, X. Liao, J. Kim, Z. Wang, O. F. N. Okello, B. Park, J. Park, C. Han, H. Heo, J. Kim, S. H. Oh, S.-Y. Choi, H. Park, and M.-H. Jo, Sci. Adv. **5**, eaaw3180 (2019).
[73]M. Marx, A. Grundmann, Y.-R. Lin, D. Andrzejewski, T. Kümmell, G. Bacher, M. Heuken, H. Kalisch, and A. Vescan, J. Electron. Mater. **47**, 910 (2018).
[74]D. Andrzejewski, M. Marx, A. Grundmann, O. Pfingsten, H. Kalisch, A. Vescan, M. Heuken, T. Kümmell, and G. Bacher, Nanotechnology **29**, 295704 (2018).
[75]J. Mun, H. Park, J. Park, D. Joung, S.-K. Lee, J. Leem, J.-M. Myoung, J. Park, S.-H. Jeong, W. Chegal, S. W. Nam, and S.-W. Kang, ACS Appl. Electron. Mater. **1**, 608 (2019).
[76]H. Cun, M. Macha, H. Kim, K. Liu, Y. Zhao, T. LaGrange, A. Kis, and A. Radenovic, Nano Res. **12**, 2646 (2019).
[77]T. Kim, J. Mun, H. Park, D. Joung, M. Diware, C. Won, J. Park, S.-H. Jeong, and S.-W. Kang, Nanotechnology **28**, 18LT01 (2017).
[78]X. Zhang, Z. Y. Al Balushi, F. Zhang, T. H. Choudhury, S. M. Eichfeld, N. Alem, T. N. Jackson, J. A. Robinson, and J. M. Redwing, J. Electron. Mater. **45**, 6273 (2016).
[79]Y.-C. Lin, B. Jariwala, B. M. Bersch, K. Xu, Y. Nie, B. Wang, S. M. Eichfeld, X. Zhang, T. H. Choudhury, Y. Pan, R. Addou, C. M. Smyth, J. Li, K. Zhang, M. A. Haque, S. Folsch, R. M. Feenstra, R. M. Wallace, K. Cho, S. K. Fullerton-Shirey, J. M. Redwing, and J. A. Robinson, ACS Nano **12**, 965 (2018).
[80]S. C. de la Barrera, Y.-C. Lin, S. M. Eichfeld, J. A. Robinson, Q. Gao, M. Widom, and R. M. Feenstra, J. Vac. Sci. Technol., B **34**, 04J106 (2016).
[81]W. Wu, C. K. Dass, J. R. Hendrickson, R. D. Montaño, R. E. Fischer, X. Zhang, T. H. Choudhury, J. M. Redwing, Y. Wang, and M. T. Pettes, Appl. Phys. Lett. **114**, 213102 (2019).
[82]R. Yue, Y. Nie, L. A. Walsh, R. Addou, C. Liang, N. Lu, A. T. Barton, H. Zhu, Z. Che, D. Barrera, L. Cheng, P.-R. Cha, Y. J. Chabal, J. W. P. Hsu, J. Kim, M. J. Kim, L. Colombo, R. M. Wallace, K. Cho, and C. L. Hinkle, 2D Mater. **4**, 045019 (2017).
[83]J. Xia, D. Zhu, L. Wang, B. Huang, X. Huang, and X.-M. Meng, Adv. Funct. Mater. **25**, 4255 (2015).
[84]X. Fan, Y. Zhao, W. Zheng, H. Li, X. Wu, X. Hu, X. Zhang, X. Zhu, Q. Zhang, X. Wang, B. Yang, J. Chen, S. Jin, and A. Pan, Nano Lett. **18**, 3885 (2018).
[85]J. Klein, A. Kuc, A. Nolinder, M. Altzschner, J. Wierzbowski, F. Sigger, F. Kreupl, J. J. Finley, U. Wurstbauer, A. W. Holleitner, and M. Kaniber, 2D Mater. **5**, 011007 (2017).
[86]S.-Y. Kim, J. H. Kim, S. Lee, J. Kwak, Y. Jo, E. Yoon, G.-D. Lee, Z. Lee, and S.-Y. Kwon, Nanoscale **10**, 19212 (2018).
[87]J. H. Kim, S.-Y. Kim, Y. Cho, H. J. Park, H.-J. Shin, S.-Y. Kwon, and Z. Lee, Adv. Mater. **31**, 1807486 (2019).
[88]C.-T. Sah, *Fundamentals of Solid State Electronics* (World Scientific Publishing Company, 1991).
[89]K. Kaasbjerg, K. S. Thygesen, and K. W. Jacobsen, Phys. Rev. B **85**, 115317 (2012).
[90]S. Mouri, Y. Miyauchi, and K. Matsuda, Nano Lett. **13**, 5944 (2013).
[91]A. M. van der Zande, P. Y. Huang, D. A. Chenet, T. C. Berkelbach, Y. You, G.-H. Lee, T. F. Heinz, D. R. Reichman, D. A. Muller, and J. C. Hone, Nat. Mater. **12**, 554 (2013).
[92]C. R. Dean, A. F. Young, I. Meric, C. Lee, L. Wang, S. Sorgenfrei, K. Watanabe, T. Taniguchi, P. Kim, and K. L. Shepard, Nat. Nanotechnol. **5**, 722 (2010).
[93]J. I.-J. Wang, Y. Yang, Y.-A. Chen, K. Watanabe, T. Taniguchi, H. O. Churchill, and P. Jarillo-Herrero, Nano Lett. **15**, 1898 (2015).
[94]H.-P. Komsa and A. V. Krasheninnikov, Phys. Rev. B **91**, 125304 (2015).
[95]W. Zhou, X. Zou, S. Najmaei, Z. Liu, Y. Shi, J. Kong, J. Lou, P. M. Ajayan, B. I. Yakobson, and J.-C. Idrobo, Nano Lett. **13**, 2615 (2013).
[96]J.-Y. Noh, H. Kim, and Y.-S. Kim, Phys. Rev. B **89**, 205417 (2014).
[97]S. Haldar, H. Vovusha, M. K. Yadav, O. Eriksson, and B. Sanyal, Phys. Rev. B **92**, 235408 (2015).
[98]B. Zhao, C. Shang, N. Qi, Z. Chen, and Z. Chen, Appl. Surf. Sci. **412**, 385 (2017).
[99]Z. G. Yu, Y.-W. Zhang, and B. I. Yakobson, Nano Lett. **15**, 6855 (2015).
[100]H. Liu, N. Han, and J. Zhao, RSC Adv. **5**, 17572 (2015).
[101]D. Liu, Y. Guo, L. Fang, and J. Robertson, Appl. Phys. Lett. **103**, 183113 (2013).
[102]C.-P. Lu, G. Li, J. Mao, L.-M. Wang, and E. Y. Andrei, Nano Lett. **14**, 4628 (2014).
[103]S. McDonnell, R. Addou, C. Buie, R. M. Wallace, and C. L. Hinkle, ACS Nano **8**, 2880 (2014).
[104]J. Yang, H. Kawai, C. P. Y. Wong, and K. E. J. Goh, J. Phys. Chem. C **123**, 2933 (2019).
[105]H. Li, M. Huang, and G. Cao, Phys. Chem. Chem. Phys. **18**, 15110 (2016).
[106]D. Ma, Q. Wang, T. Li, C. He, B. Ma, Y. Tang, Z. Lu, and Z. Yang, J. Mater. Chem. C **4**, 7093 (2016).
[107]H. Nan, Z. Wang, W. Wang, Z. Liang, Y. Lu, Q. Chen, D. He, P. Tan, F. Miao, and X. Wang, ACS Nano **8**, 5738 (2014).
[108]J. Jiang, R. Pachter, and S. Mou, Nanoscale **10**, 13751 (2018).
[109]Y. J. Zheng, Y. Chen, Y. L. Huang, P. K. Gogoi, M.-Y. Li, L.-J. Li, P. E. Trevisanutto, Q. Wang, S. J. Pennycook, A. T. S. Wee, and S. Y. Quek, ACS Nano **13**, 6050 (2019).
[110]S. Zhang, C.-G. Wang, M.-Y. Li, D. Huang, L.-J. Li, W. Ji, and S. Wu, Phys. Rev. Lett. **119**, 046101 (2017).
[111]Y. Guo, D. Liu, and J. Robertson, Appl. Phys. Lett. **106**, 173106 (2015).
[112]R. Addou and R. M. Wallace, ACS Appl. Mater. Interfaces **8**, 26400 (2016).
[113]D. Ma, B. Ma, Z. Lu, C. He, Y. Tang, Z. Lu, and Z. Yang, Phys. Chem. Chem. Phys. **19**, 26022 (2017).
[114]M. Tosun, L. Chan, M. Amani, T. Roy, G. H. Ahn, P. Taheri, C. Carraro, J. W. Ager, R. Maboudian, and A. Javey, ACS Nano **10**, 6853 (2016).
[115]J. Kwak, Y. Jo, S. Song, J. H. Kim, S.-Y. Kim, J.-U. Lee, S. Lee, J. Park, K. Kim, G.-D. Lee, J.-W. Yoo, S. Y. Kim, Y.-M. Kong, G.-H. Lee, W.-G. Lee, J. Park, X. Xu, H. Cheong, E. Yoon, Z. Lee, and S.-Y. Kwon, Adv. Mater. **30**, 1707260 (2018).
[116]S. Song, S.-Y. Kim, J. Kwak, Y. Jo, J. H. Kim, J. H. Lee, J.-U. Lee, J. U. Kim, H. D. Yun, Y. Sim, J. Wang, D. H. Lee, S.-H. Seok, T.-I. Kim, H. Cheong, Z. Lee, and S.-Y. Kwon, Adv. Sci. **6**, 1801370 (2019).
[117]D. Kiriya, M. Tosun, P. Zhao, J. S. Kang, and A. Javey, J. Am. Chem. Soc. **136**, 7853 (2014).
[118]H.-M. Li, D. Lee, D. Qu, X. Liu, J. Ryu, A. Seabaugh, and W. J. Yoo, Nat. Commun. **6**, 6564 (2015).
[119]M. S. Choi, D. Qu, D. Lee, X. Liu, K. Watanabe, T. Taniguchi, and W. J. Yoo, ACS Nano **8**, 9332 (2014).
[120]D.-H. Kang, M.-S. Kim, J. Shim, J. Jeon, H.-Y. Park, W.-S. Jung, H.-Y. Yu, C.-H. Pang, S. Lee, and J.-H. Park, Adv. Funct. Mater. **25**, 4219 (2015).
[121]K. Dolui, I. Rungger, C. D. Pemmaraju, and S. Sanvito, Phys. Rev. B **88**, 075420 (2013).
[122]J. Suh, T.-E. Park, D.-Y. Lin, D. Fu, J. Park, H. J. Jung, Y. Chen, C. Ko, C. Jang, Y. Sun, R. Sinclair, J. Chang, S. Tongay, and J. Wu, Nano Lett. **14**, 6976 (2014).
[123]S. Y. Wang, T. S. Ko, C. C. Huang, D. Y. Lin, and Y. S. Huang, Jpn. J. Appl. Phys. **53**, 04EH07 (2014).
[124]K. Zhang, B. M. Bersch, J. Joshi, R. Addou, C. R. Cormier, C. Zhang, K. Xu, N. C. Briggs, K. Wang, S. Subramanian, K. Cho, S. Fullerton-Shirey, R. M. Wallace, P. M. Vora, and J. A. Robinson, Adv. Funct. Mater. **28**, 1706950 (2018).
[125]Q. Yue, S. Chang, S. Qin, and J. Li, Phys. Lett. A **377**, 1362 (2013).
[126]P. Zhao, D. Kiriya, A. Azcatl, C. Zhang, M. Tosun, Y.-S. Liu, M. Hettick, J. S. Kang, S. McDonnell, S. KC, J. Guo, K. Cho, R. M. Wallace, and A. Javey, ACS Nano **8**, 10808 (2014).
[127]H. Fang, M. Tosun, G. Seol, T. C. Chang, K. Takei, J. Guo, and A. Javey, Nano Lett. **13**, 1991 (2013).
[128]L. Yu, A. Zubair, E. J. G. Santos, X. Zhang, Y. Lin, Y. Zhang, and T. Palacios, Nano Lett. **15**, 4928 (2015).

[129]X. Duan, C. Wang, Z. Fan, G. Hao, L. Kou, U. Halim, H. Li, X. Wu, Y. Wang, J. Jiang, A. Pan, Y. Huang, R. Yu, and X. Duan, Nano Lett. **16**, 264 (2016).
[130]H.-J. Chuang, B. Chamlagain, M. Koehler, M. M. Perera, J. Yan, D. Mandrus, D. Tomanek, and Z. Zhou, Nano Lett. **16**, 1896 (2016).
[131]T. Wang, K. Andrews, A. Bowman, T. Hong, M. Koehler, J. Yan, D. Mandrus, Z. Zhou, and Y.-Q. Xu, Nano Lett. **18**, 2766 (2018).
[132]P. Yu, J. Lin, L. Sun, Q. L. Le, X. Yu, G. Gao, C.-H. Hsu, D. Wu, T.-R. Chang, Q. Zeng, F. Liu, Q. J. Wang, H.-T. Jeng, H. Lin, A. Trampert, Z. Shen, K. Suenaga, and Z. Liu, Adv. Mater. **29**, 1603991 (2017).
[133]Y.-H. Lee, X.-Q. Zhang, W. Zhang, M.-T. Chang, C.-T. Lin, K.-D. Chang, Y.-C. Yu, J. T.-W. Wang, C.-S. Chang, L.-J. Li, and T.-W. Lin, Adv. Mater. **24**, 2320 (2012).